Recovering lateral variations in lithospheric strength from bedrock motion data using a coupled ice sheet-lithosphere model

J. van den Berg,[1] R. S. W. van de Wal,[1] and J. Oerlemans[1]

Received 19 April 2005; revised 20 December 2005; accepted 24 January 2006; published 27 May 2006.

[1] A vertically integrated two-dimensional ice flow model was coupled to an elastic lithosphere-Earth model to study the effects of lateral variations in lithospheric strength on local bedrock adjustment. We used a synthetic bedrock profile and a synthetic climate to model a characteristic ice sheet through an ice age cycle. Realistic differences in lithospheric strength altered the local bedrock adjustment up to 100 m, the ice extent by tens of kilometers, and the ice volume by several percent. Hence, when modeling ice sheets, it is essential to include information on lithospheric structure. In addition, we used the coupled ice flow–lithosphere model to construct synthetic bedrock motion time series to assess their potential in resolving lithospheric structure. Inverse experiments showed that the model can resolve lateral variations in lithospheric strength from these bedrock motion time series, provided that we have data from both sides of a lateral transition in lithospheric strength. The inversion that solved for a lateral transition was able to find a solution that was consistent with all data, even if they were noisy. In the presence of lateral variations in lithospheric strength, there was no solution to the inverse problem for which all data were modeled correctly by a uniform lithospheric model. The synthetic data showed no significant sensitivity to the location of the transition. Hence we require information from independent sources, such as seismology or gravity, about the locations of transitions in lithospheric strength.

Citation: van den Berg, J., R. S. W. van de Wal, and J. Oerlemans (2006), Recovering lateral variations in lithospheric strength from bedrock motion data using a coupled ice sheet-lithosphere model, *J. Geophys. Res.*, *111*, B05409, doi:10.1029/2005JB003790.

1. Introduction

[2] To understand the Earth's climate and to predict future climate change, it is essential to study the sensitivity of the Earth's system to change. The growth and decay of large ice sheets were amongst the largest climate changes in the past million years. The physical processes controlling the evolution of ice sheets are generally studied with dynamical ice flow models. Most studies consider the response of the ice to the upper boundary conditions, i.e., climate and sea level. However, in this paper we focus on the lower boundary, i.e., the lithosphere.

[3] Bending of the outer layers of the Earth as response to the added weight of ice results in a isostatic adjustment of the bedrock of up to one third of the ice thickness. This effect influences surface temperature, basal topography, and the stress field in the ice. To calculate the ice evolution as accurately as possible, dynamical ice flow models incorporate this vertical displacement by assuming an Earth rheology. *Le Meur and Huybrechts* [1996] have shown that a simple Earth model, namely a purely elastic lithosphere with uniform thickness and strength underlain by a uniform mantle with a single relaxation time, works reasonably well compared to more realistic, but also computationally more demanding, viscoelastic Earth models, with several laterally uniform layers.

[4] However, seismological and gravitational methods have suggested large lateral differences in lithospheric structure [*Djomani et al.*, 1999; *Bannister et al.*, 2003; *Darbyshire et al.*, 2004; *Pérez-Gussinye and Watts*, 2005]. For example, there are strong indications for a large transition under the Trans Antarctic Mountains from weak lithosphere in the western part of the continent to strong lithosphere in the eastern part [*Stern and Ten Brink*, 1989; *Bannister et al.*, 2003]. Seismological and gravitational methods are very useful in retrieving information on lithospheric structure, but they have some drawbacks as well. For instance, seismological data are difficult to interpret in terms of actual strength, since lithospheric strength is a function of composition, structure, and tectonic history [*Braitenberg et al.*, 2002]. Gravitational methods experience difficulties when the bedrock is not in isostatic equilibrium, or if the load is not well known or highly variable, for example in regions with a glaciation history.

[1] Institute for Marine and Atmospheric Research, University of Utrecht, Utrecht, Netherlands.

Copyright 2006 by the American Geophysical Union.
0148-0227/06/2005JB003790$09.00

[5] To be able to use gravitational methods in (formerly) glaciated regions, an ice history, such as ICE-3G and its descendants, was constructed from glacial isostatic adjustment data [e.g., *Tushingham and Peltier*, 1991; *Milne et al.*, 2002]. This ice history was then assumed to be a known loading history to study the rheological properties of the Earth [e.g., *Wolf*, 1993; *Vermeersen and Sabadini*, 1999; *Di Donato et al.*, 2000; *Kaufmann and Wu*, 2002]. Such an ice history is derived from (mostly sea level) observations and does not include ice mechanics.

[6] Recently, experiments have been performed using these ice loading histories on the occurrence of possible lateral transitions in lithospheric strength. For example, *Kaufmann et al.* [2000], *Kaufmann and Wu* [2002], and *Zhong et al.* [2003] have experimented with the effects of lateral variations in lithospheric strength on local glacial isostatic adjustment data. *Kaufmann et al.* [2000] concluded that realistic lateral variations in strength underneath these prescribed ice loads (no ice dynamics) could give differences in local sea level data up to 10 m. *Kaufmann et al.* [2005] showed that modeled isostatic adjustments strongly depended on the chosen ice history. In this latter paper one of the ice histories was based on a dynamical ice flow model. To resolve lateral variations in lithospheric strength both *Kaufmann and Wu* [2002] and *Zhong et al.* [2003] proposed an inverse procedure with several laterally homogeneous models and local data. Variations in local estimates between different regions indicated variations in lithospheric structure. In this paper we present a new approach to retrieve information on lateral variations in lithospheric strength. This new method is based on the addition of a dynamical ice flow model to the inverse procedure.

[7] Usually, ice evolution in a dynamical ice flow model is forced by a climate model. Such a climate model is derived from isotope measurements from ice and/or ocean sediment cores. This procedure is completely independent from the glacial isostatic adjustment data ice histories, such as ICE-3G. Moreover, the ice thickness distribution in these ice histories is generally based on optimization procedures, whereas dynamical ice flow models use a description of ice rheology. Hence ice histories, such as ICE-3G, and dynamical ice flow models differ in both the underlying data set and the modeling approach. Therefore dynamical ice flow models provide an additional, independent source of information, which can be used to invert for lithospheric structure.

[8] As mentioned before, dynamical ice flow models need to include isostatic adjustment calculations to reach the most accurate understanding of the ice thickness and extent throughout glacial cycles. Therefore we constructed a new dynamically fully coupled ice sheet–Earth model. We used a relatively simple Earth model based on a purely elastic lithosphere including lateral variations in strength underlain by a uniform mantle with a single relaxation time as described in section 2. This Earth model was coupled to an ice model based on the shallow ice approximation as described in section 3. Section 4 shows a characteristic ice sheet evolution for three different Earth models to illustrate the full model. This ice-Earth model was then used in a synthetic approach to assess an inverse procedure to resolve lateral variations in lithospheric strength from vertical isostatic bedrock adjustment data (section 5).

2. Lithospheric Model

[9] The response of the solid Earth to an ice load can to first order be described by the bending or flexure of an elastic lithosphere combined with a time delay due to the viscous properties of the mantle below. If we assume that the elastic properties and the thickness of the lithosphere are constant throughout the plate, the behavior of the lithosphere can be described by a well-known fourth-order differential equation [e.g., *Turcotte and Schubert*, 2002; *Van der Veen*, 1999; *Brotchie and Silvester*, 1969], which can be solved analytically for a given load, q_{load}:

$$D\nabla^4 w - q = 0, \tag{1}$$

where w is the vertical deflection, ∇ is the two-dimensional biharmonic operator, $q = q_{load} - \rho_m g w$ is the load minus the buoyancy of the mantle, and D is called the flexural rigidity and is a measure for the strength of the lithosphere. This is defined as

$$D = \frac{Eh^3}{12(1-\nu^2)}, \tag{2}$$

where h is the thickness of the elastic lithosphere, and E and ν are elastic parameters, respectively Young's modulus and Poisson's ratio.

[10] For the general case where the elastic properties are not homogeneous, we cannot use the standard flexural equation presented in equation (1). For those cases we have to use a more general equation (see Appendix A for more details),

$$(\mathbf{L}\nabla)^T \mathbf{D}' \mathbf{L}\nabla w - q = 0, \tag{3}$$

where $(\mathbf{L}\nabla)$ is given by

$$(\mathbf{L}\nabla) = \left[\frac{\partial^2}{\partial x^2} \quad \frac{\partial^2}{\partial y^2} \quad 2\frac{\partial^2}{\partial x \partial y} \right]^T, \tag{4}$$

and the matrix $\mathbf{D}'$ is given by

$$\mathbf{D}' = D \begin{bmatrix} 1 & \nu & 0 \\ \nu & 1 & 0 \\ 0 & 0 & (1-\nu)/2 \end{bmatrix}, \tag{5}$$

Note that when D is constant, equation (3) reduces to equation (1); see also equation (A19) in Appendix A, which is the equivalent of equation (3) without the matrix notation.

[11] As we are interested in lateral variations in lithospheric strength we use equations (3) to (5) to describe the vertical motion of the lithosphere.

[12] Equations (3) to (5) describe an instantaneous elastic response. The Earth however cannot respond instantaneously, since the mantle below has a nonzero viscosity.

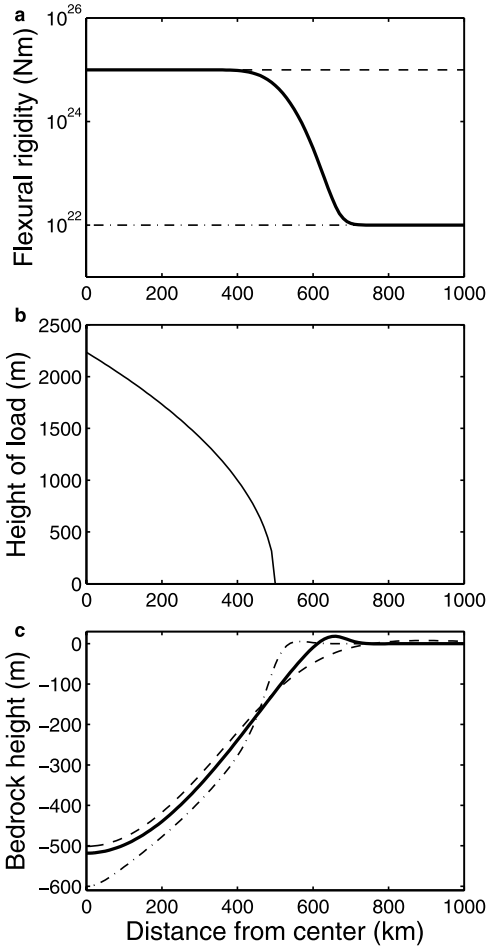

Figure 1. (a) Flexural rigidity as a function of distance from the center. (b) Height of load as a function of distance from the center. (c) Deflection as a function of distance from the center. The dashed and dash-dotted lines represent the analytical solutions for $D = 10^{25}$ Nm and $D = 10^{22}$ Nm, respectively.

Therefore the temporal response has a time delay and is calculated as [e.g., *Van der Veen*, 1999]

$$\frac{\partial b}{\partial t} = -\frac{1}{\tau}(b + w - b_0). \tag{6}$$

This is a simple first-order approach in which we characterize the response of the mantle with one single relaxation time τ, commonly used in glaciological applications with a value of 3000 years. The parameter w is the total subsidence as calculated by the lithospheric model, b is the height of the bedrock, and b_0 is the initial topography, hence topography without ice. The Earth was not adjusted each time step of the ice model, but every ten years instead. This is allowed, since this is much less than τ.

2.1. Numerical Properties of the Lithospheric Model

[13] We have numerically solved equation (3) on a square equidistant grid with first-order central differencing, resulting in a completely implicit procedure. At the boundaries we set the deflection w as well as its gradient over that specific boundary to zero.

[14] We performed several discretization tests for varying grid point distances. For coarse grids ($\Delta x > 40$ km), the solution was inaccurate. For fine grids ($\Delta x < 20$ km), the solutions were numerically unstable because the ice sheet surface was too smooth to calculate surface derivatives up to fourth order within machine precision. Therefore we used a grid point distance Δx of 30 km. Note that these results are valid for the typically smooth, large ice sheets we used in this manuscript. For specific applications the grid requirements could be different.

[15] We know from the analytical solution to equation (1) that the response of the lithosphere to an arbitrary load is characterized by a large deflection underneath the load and a positive, and small peripheral bulge outside the load. The total vertical movement is controlled by the flexural rigidity (D). Since the boundary conditions require that the deflection is zero at the boundaries of the domain, the calculated deflections are valid as long as the domain boundaries are after the bulge, where the deflections are very small. For this reason we used a domain of 3000 by 3000 km where the ice load never had a radius larger than approximately 600 km.

[16] In this paper we modeled transitions in flexural rigidity over several orders of magnitude. Several tests with varying taper lengths showed that these very large transitions require a horizontal scale of approximately 300 km width to avoid numerical instabilities. As our interest is in the continental scales, this is not a severe restriction.

2.2. Response of the Lithosphere to a Parabolic Load

[17] As an example of the lithospheric part of the algorithm we show the response of three lithospheric models to a radially symmetric parabolic load with a radius of 500 km (Figure 1b). Figure 1a shows the flexural rigidities of the three lithospheric models. We used two lithospheric models with a constant flexural rigidity; one with $D = 10^{22}$ Nm (a typical value for oceanic lithosphere) and one with $D = 10^{25}$ Nm (a typical value for strong, continental lithosphere). The third model contained a transition with a width of 300 km from $D = 10^{25}$ Nm to $D = 10^{22}$ Nm, with the center of the transition at a radial distance of 500 km. As such, the ice margin is directly located above the transition. This corresponds to a situation where the ice margin is positioned on the transition from continental to oceanic lithosphere. The transition is modeled with a combination of two error functions, characterized by a rapid change followed by a more gradual asymptotic behavior toward the final values. Figure 1c shows the resulting deflections as a function of distance. We see differences up to 100 m between the solutions. Underneath the load the curve for the variable lithosphere resembles the one for the strong lithosphere, which makes sense since the transition only occurs at 500 km distance from the center. At the transition however, the curve for the variable lithosphere shifts toward the one for the weak lithosphere; the bulge moves closer to the margin of the load and is higher than for both other curves. These results are generally in agreement with *Kaufmann et al.* [2000] and *Kaufmann and Wu* [2002]. The result implies

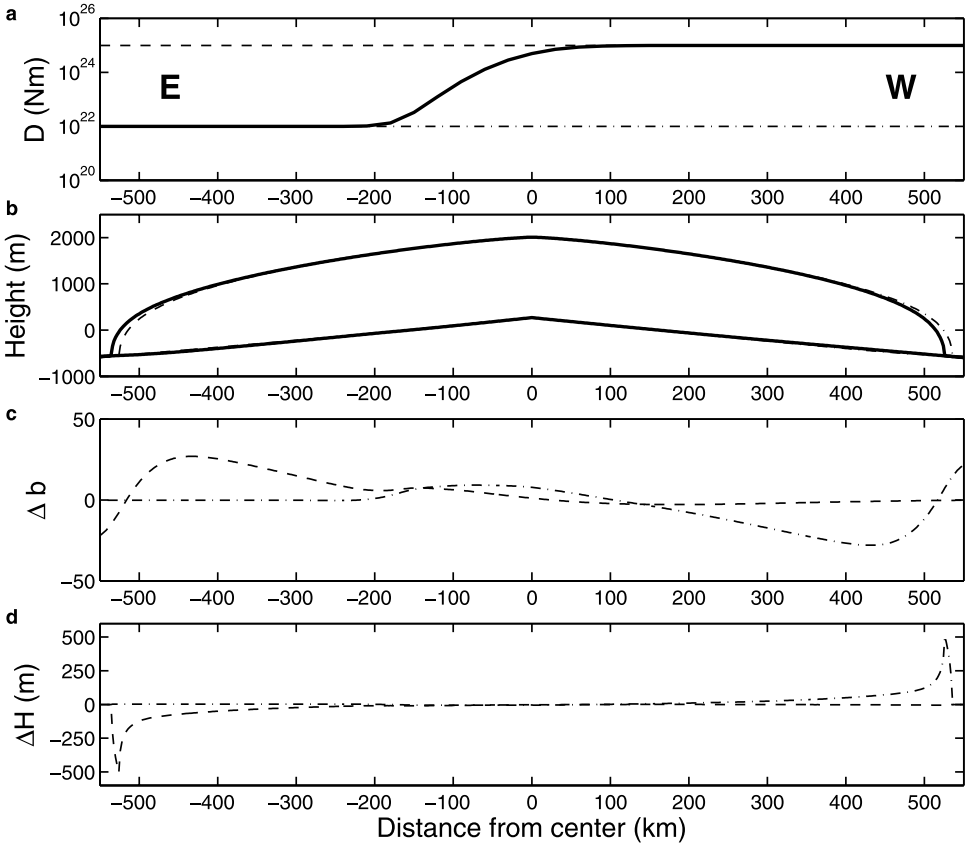

Figure 2. Results after 100,000 years of ice growth. (a) Flexural rigidity for the three lithospheric models: the variable rigidity (solid line), $D = 10^{22}$ Nm (dash-dotted line), and $D = 10^{25}$ Nm (dashed line). (b) West-east cross section of an ice sheet at LGM. (c) Differences in bedrock height of the constant lithospheric model with the variable lithospheric models, i.e., $b_{constant} - b_{variable}$, as a function of distance from the center along the cross section. (d) Similar to Figure 2c but now for ice thickness differences.

that the possible magnitude of a peripheral bulge strongly depends on the lateral variation in lithospheric strength.

3. Ice Model

[18] The ice model is based on the vertically integrated continuity equation [e.g., *Van der Veen*, 1999]:

$$\frac{\partial H}{\partial t} = -\nabla \cdot (H\,\mathbf{U}) + B \tag{7}$$

where H is the ice thickness, $\mathbf{U}$ is the vertically averaged horizontal velocity, and B is the mass balance, which is the net increase or decrease of local ice thickness in meters of ice per unit time due to snow fall or ice melt at the surface of the ice sheet. We used the shallow ice approximation [e.g., *Hutter*, 1983; *Van der Veen*, 1999], which assumes that the horizontal extent is much larger than the ice thickness. For a two-dimensional model without sliding, the expression for the vertical mean horizontal velocity reduces to the deformation velocity, which is given by

$$\mathbf{U} = \frac{-2}{n+2}(\rho_i g)^n A \left[\frac{\partial h_s}{\partial x}^2 + \frac{\partial h_s}{\partial y}^2\right]^{\frac{n-1}{2}} \nabla h_s\, H^{n+1}, \tag{8}$$

where h_s is the surface height, ρ_i is the ice density, g the gravitational acceleration, and A and n are rheological parameters, where n is set to 3. The parameter A is assumed to be constant throughout the ice.

[19] A good first-order approximation for the mass balance is a linear profile for which the only variable is height above a reference level;

$$B = \min(B_{\max}, \beta(h_s - ELA)) \tag{9}$$

where β is the mass balance gradient in yr^{-1} and ELA the equilibrium line altitude in meters. In general temperatures decrease with increasing altitude. We assume that the total precipitation is constant with altitude. The slope of the mass balance profile is then caused by the net effect of decreasing melt with altitude and the simultaneous increase of the snow fraction of the precipitation. The part of the profile where B approaches the value $B_{\max}$ reflects the absence of melt at high elevations where all precipitation falls as snow. At the ELA the mass balance is zero, hence no net change in ice thickness due to accumulation or melt.

[20] We solved the system, given by equations (7) to (9), on a two-dimensional equidistant square grid with central differencing in the spatial domain and a grid point distance of 2 km for a total domain of 1500 by 1500 kilometers. The

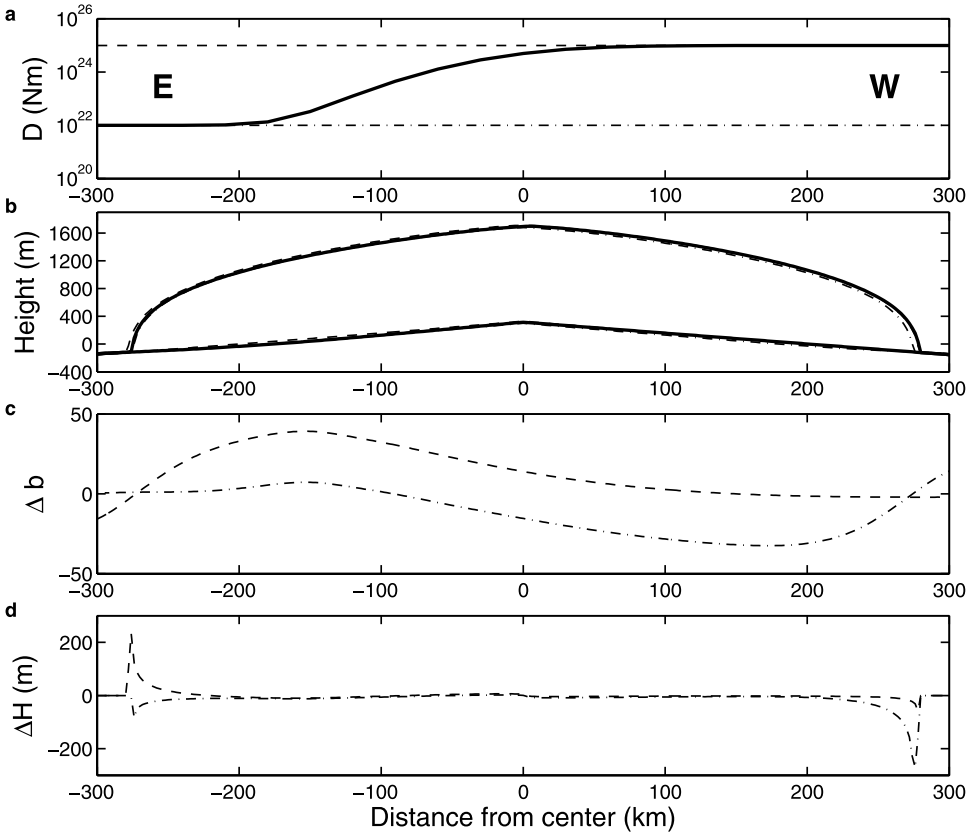

Figure 3. Results after 20,000 years of deglaciation. (a) Flexural rigidity for the three lithospheric models: the variable rigidity (solid line), $D = 10^{22}$ Nm (dash-dotted line), and $D = 10^{25}$ Nm (dashed line). (b) West-east cross section of an ice sheet at PD. (c) Differences in bedrock height of the constant lithospheric model with the variable lithospheric models, i.e., $b_{constant} - b_{variable}$, as a function of distance from the center along the cross section. (d) Similar to Figure 3c but now for ice thickness differences.

model corresponds to the type II ice models from the EISMINT experiments [*Huybrechts et al.*, 1996], which is widely used by ice sheet modelers. For the time integration an alternating direction implicit (ADI) method is used [e.g., *Mahaffy*, 1976; *Huybrechts*, 1992]. The ice thickness at all boundaries is set to zero.

[21] The grid point distance and the domain size are not the same as for the lithospheric model. We required a fine grid for the ice to be calculated accurately. For details, see *van den Berg et al.* [2006]. To obtain the response for a grid point in the Earth domain, we applied an average of the overlapping grid points in the ice domain. Once the Earth response was calculated, we interpolated the calculated bedrock elevation using bicubic splines to the ice domain. This procedure works as long as the bedrock response is a smooth function of x and y.

4. A Coupled Synthetic Ice Sheet–Bedrock Evolution

[22] To illustrate the combined effect of the ice and lithosphere model, we considered the development of an ice sheet over a period of 100,000 years followed by partial melt over a period of 20,000 years. We used three lithospheric models: two models with a constant rigidity; one weak lithosphere with $D = 10^{22}$ Nm, and one strong lithosphere with $D = 10^{25}$ Nm. The third lithospheric model contained a transition of 300 km width from $D = 10^{22}$ Nm in the western (or left) half of the domain to $D = 10^{25}$ Nm in the eastern (or right) half of the domain (Figures 2a and 3a). This synthetic geometry was inspired by the geological structure of Antarctica, where there are strong indications for a transition between weak lithosphere west of the Trans Antarctic Mountains (TAM) and strong lithosphere to the east. The values for the flexural rigidity are representative for that transition [*Stern and Ten Brink*, 1989].

[23] We prescribed the initial bedrock profile as

$$b_0(r) = b_{\max} - \gamma r, \tag{10}$$

with b_0 the initial bedrock height in meters, $b_{\max}$ the maximum initial bedrock height, γ the initial bedrock gradient, and $r = \sqrt{x^2 + y^2}$ the distance from the center in kilometers. The parameterization of the mass balance as an altitude-dependent parameter requires the introduction of a surface slope. Without the surface slope, the ice model is numerically unstable.

[24] Table 1 shows the parameter values for this experiment. In spite of the lithospheric model, the prescribed mass balance profile is not inspired by the climate on Antarctica, making this a purely theoretical experiment. The equilibrium line altitude *ELA* was 150 m during the first 100,000 years.

Table 1. Parameters for the Experiments[a]

Parameter	Value
β, yr^{-1}	0.005
ELA, m	150 (first 100,000 years), 500 (final 20,000 years)
B_{max}, m yr^{-1}	0.1
τ, years	3000
b_{max}, m	400
γ, m km^{-1}	1.3

[a]Here β is the mass balance gradient, ELA is the altitude where the mass balance is zero, B_{max} is the maximum mass balance, τ is the characteristic relaxation time for the mantle, b_{max} is the highest point in the bedrock topography without ice, and γ is the gradient in the bedrock topography without ice.

Results are presented in Figure 2. Figure 2b shows an east-west profile through the domain at this time, which we will call Last Glacial Maximum (LGM). After these 100,000 years *ELA* was consecutively moved up to 500 m for a duration of 20,000 years. Figure 3 shows the results after this deglaciation. Figure 3b shows an east-west profile through the domain after this total of 120,000 years, which we will call present day (PD). Note that these profiles are not steady state profiles, but time slices. Figures 2c and 3c show the differences in bedrock heights between the different Earth models. Figures 2d and 3d show the resulting differences in ice thickness.

[25] For the case with the variable lithosphere, the ice sheet resembles the ice sheet for the weak lithosphere on the weak part of the domain. On the strong part of the domain, the ice sheet resembles the ice sheet for the strong lithosphere. In the center of the domain the differences with the variable lithospheric model are smallest for the strong lithosphere. Since strong lithosphere has a larger region of influence (or larger flexural wavelength) than weak lithosphere, the strong part of the lithosphere dominates the transition region.

[26] Fast melting occurs during the final 20,000 years of the cycle (Figure 3). The ice decreases more rapidly in ice extent than in ice thickness. The resulting ice sheet is almost as large as the transition in rigidity itself. As a result, the transition is much more noticeable in the bedrock response, giving more widespread differences between the three lithospheric models.

[27] The ice extent is different for each Earth model, causing the differences in ice height to be 100 m or more in the sensitive marginal areas. The differences in ice extent for the realistic strengths used in Figure 2 and 3 are tens of kilometers, making this an important feature. This marks the importance for ice modeling of taking into account the dynamical response of the ice to the strength of the lithosphere.

[28] Figure 4 shows the corresponding bedrock height change for specific locations as a function of time together with the resulting ice volume. Differences in bedrock deflection between the different lithospheric models are approximately 20–30%. We observe that not only the ice extent, but also the ice volume is a function of lithospheric strength. Differences in lithospheric strength lead to differences in resulting ice volume of up to ten percent. We performed tests with different ice rheologies by varying the flow parameter A by 30%. This did not influence these relative volume differences between the different Earth models. Varying the climate parameters such as the mass balance β and the maximum mass balance gradient B_{max} did not have a large effect either. Again, this clearly marks the importance of taking into account the dynamical coupling between ice and Earth for the modeling of ice. Not just taking into account changes in the rigidity, but also knowing the absolute value of the strength is important.

5. Reconstruction of Lithospheric Strength From Synthetic Bedrock Data

[29] Relative sea level curves contain both the signals from actual sea level changes and information about the bedrock motion. Close to the ice sheet they contain information on the flexural behavior of the lithosphere [e.g., *Milne et al.*, 2002]. The use of these data requires coupling of the dynamical models presented here to a full gravitational sea level model. We assume that we can extract the

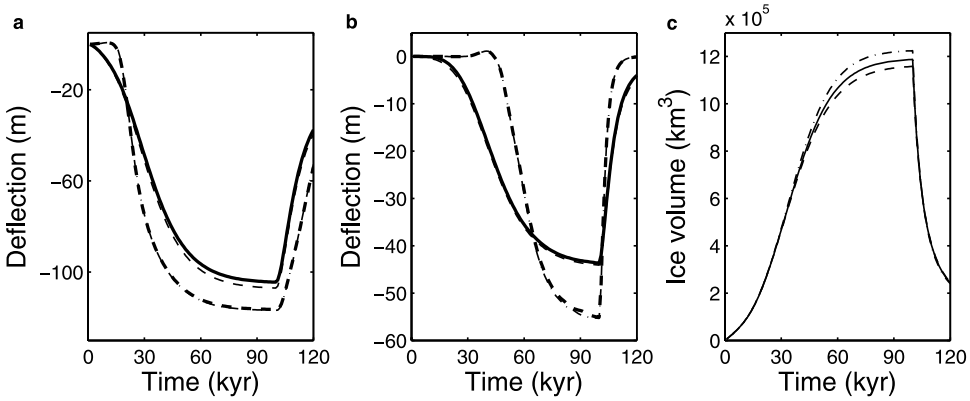

Figure 4. (a) Bedrock data at 250 km distance from the center for the eastern part of the variable lithosphere (thick solid line), the western part of the variable lithosphere (thick dashed line), and the two constant lithospheres (strong, thin dashed line, and weak, dash-dotted line). (b) Same as Figure 4a but for a distance of 500 km from the center. (c) Ice volume curve for the variable lithosphere and the two constant lithospheres (dash-dotted line and dashed line).

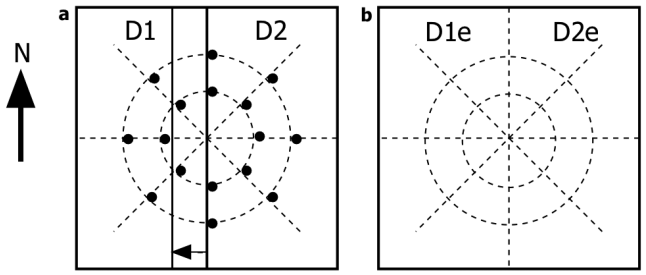

Figure 5. Geometry of the inversion. (a) Geometry of the true model with $D1 = 10^{22}$ Nm and $D2 = 10^{25}$ Nm. Figure 5a also shows the locations of the bedrock data in eight directions from the center (north, northeast, east, southeast, south, southwest, west, and northwest) and at two distances from the center (r = 250 and 500 km). In total, there are 16 bedrock curves as a function of time. (b) Geometry of the inversion. We invert for two parameters ($D1e$ and $D2e$). The generated bedrock data are in the same locations as in Figure 5a.

isostatic adjustment of the bedrock from the sea level curves. Hence we only use the data of the bedrock motion and perform several experiments to assess their ability to provide information on lithospheric strength.

[30] The climate, initial bedrock topography, and calculated bedrock height yield the ice thickness. This is in turn input for the bedrock model. The output from the bedrock model is bedrock height, which is used for the next time step in the ice model and so on. Note the dynamical coupling between ice and Earth. In the following experiments the climate and initial bedrock topography are assumed to be known and fixed to the values of the previous section, presented in Table 1. The data are given by the resulting bedrock height time series. This leaves only the lithospheric strength model as unknown parameter, which we aim to recover from the bedrock height data. The ice sheet responds both to climate and to the lithosphere, hence will differ in ice thickness and extent for different lithospheric models, as shown in section 4.

[31] Figure 5a shows the "true" synthetic geometry of the lithosphere, with an eastern and western value for D with the transition in the center of the continent (as indicated by the thick solid line in the center of the domain), which we aim to recover from synthetic bedrock data. We used a square domain with a transition from weak to strong lithosphere in the center, such that the western part of the domain is weak ($D1 = 10^{22}$ Nm), and the eastern part is strong ($D2 = 10^{25}$ Nm). The transition width is 300 km. Figure 5a also shows a thin, vertical, solid line and an arrow. We will come back to this in section 5.2.1.

[32] For this true lithospheric strength model we created the true bedrock response data d^t. Figure 5a shows the locations; we took data d^t from eight directions (north, northeast, east, southeast, south, southwest, west, and northwest) and at two distances from the center (250 and 500 km). In total we generated 16 bedrock height curves as a function of time. A data point was calculated every 1000 years, hence we generated 120 data points for each location for the glacial-interglacial run of 120 kyr. We only used the last 20 time points of the total 120, since these are from the deglaciation part of the curves, which in practice is the only part of the bedrock curves we may expect to be available from real observations.

5.1. Single Strength Inversion

[33] In the first experiment we investigated whether we could find a single strength for the entire continent (Figure 5b, $D1e = D2e = De$) which provides approximately the same bedrock adjustment data as obtained from the true lithospheric strength model with a transition from weak to strong lithosphere. We modeled bedrock adjustment data d^e for several single strengths De at the same times and locations as the true data d^t. We then compared these different data d^e with the true data d^t. For the comparison we used a cost function based on the χ-square test:

$$\chi^2 = \frac{1}{N\,T}\sum_n \sum_k \left(\frac{\left(d^t_{n,k} - d^e_{n,k}\right)^2}{\left(\sigma^t_{n,k}\right)^2} \right) \tag{11}$$

where the sum n is over all the data locations ($N = 16$) and the sum k is over all times ($T = 20$). The value for χ^2 is different for each single strength De and has a minimum for that value of De where the modeled bedrock data d^e are closest to the true data d^t. Once χ^2 is equal to one, the modeled bedrock data d^e match the true data d^t within one standard deviation.

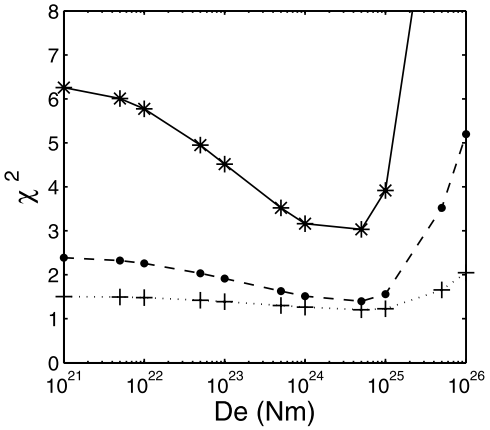

Figure 6. The χ^2 distribution as a function of De for bedrock data for 5% noise (solid line), 10% noise (dashed line), and 20% noise (dotted line).

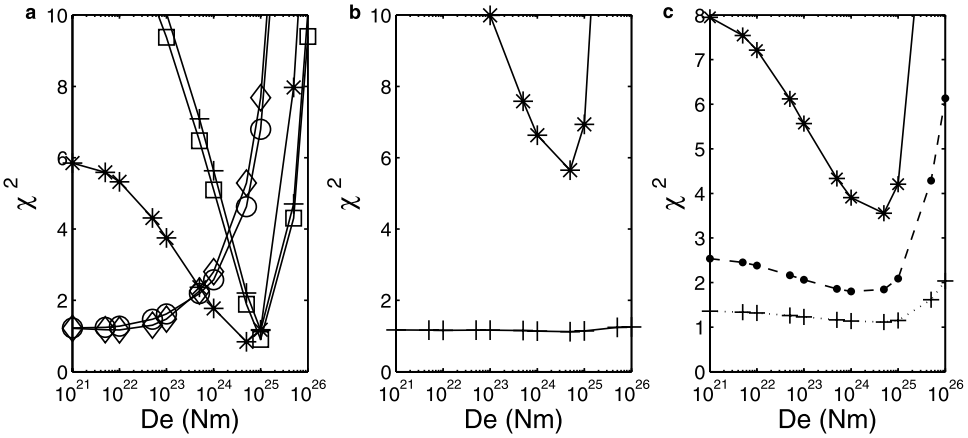

Figure 7. The χ^2 distribution as a function of *De* for the bedrock data with 5% noise. (a) Cost function when all data in one specific direction (stars for north, pluses for northeast, squares for east, circles for southwest, and diamonds for west) are used. (b) Misfit when all data at specific distances are used (stars for 250 km and pluses for 500 km). (c) Similar to Figure 6, but now the estimates *De* are calculated with a prescribed ice history.

5.1.1. Results

[34] Figure 6 shows χ^2 as a function of *De* for an addition of either 5, 10, or 20% Gaussian noise in the true data d^t. The resulting best estimate *De* is roughly at the average of both true rigidities. An uncertainty of 20% is not uncommon for sea level data, but the resulting estimate for the lithospheric strength is quite robust; the minimum in misfit remains significant.

[35] Figure 7a shows χ^2 for data from a specific direction only. We do not show results from the southeast and the northwest, because these data are the same for the northeast and the southwest respectively due to symmetry. The data from the western part of the domain yield as best estimate for *De* the true value *D*1. Similarly, for data from the eastern part of the domain, the best estimate for *De* is equal to the true value *D*2. If the direction is not perpendicular (i.e., northeast or southwest) to the transition, the resulting best estimate *De* does not change much compared to the perpendicular directions east and west; the strong estimate is not affected, the weak estimate is a little different, but the minimum is very flat, which is a result of the logarithmic scale. When the data from the north are used, we find the average between *D*1 and *D*2. This value is also equal to the local value, but it is not possible to distinguish whether the result is based on the local value or the average. The values of χ^2 in Figure 7a do approach one unlike the values for low noise levels in Figure 6. This implies that there is no single value *De* for the entire domain for which data on both sides of the transition are modeled well. This means that it is not possible to perform a good inversion for a single strength in a consistent model if the true situation has a variable lithospheric strength.

[36] Figure 7b shows χ^2 for data from one distance only, but using all directions. The curve with the clearest minimum is the one for a distance of 250 km from the center. The bedrock at these locations is covered by ice for a large part of the ice history, but is located near the ice margin for the present-day situation (Figure 3). Further from the margin, not much happened to the bedrock, hence a value for χ^2 close to one, but also hardly a minimum. This implies that, as expected, we need data as close to the ice as possible in order to discriminate between several values for lithospheric strength.

5.1.2. Effects of Uncertainties in the Ice and Earth Model

[37] To assess the effects of uncertainties in the ice model, we also performed the experiment without the full dynamical coupling of ice and lithosphere. To acquire an ice history, we calculated, with the dynamical coupling, for a uniform lithospheric strength the corresponding ice sheet evolution. For this specific ice history, we saved the ice thicknesses every 500 years. These ice thicknesses were then used as a prescribed ice history. Hence the modeled bedrock adjustment data d^e for each lithospheric strength *De* now shared the same input, namely this ice history prescribed every 500 years, instead of the dynamically corresponding ice sheet. This procedure did not influence the true data d^t, these were kept the same as in the previous experiments. Only the estimates *De* were assessed with the new ice history.

[38] Figure 7c shows the resulting χ^2 for an ice history corresponding to a lithospheric strength *De* of 10^{22} Nm. We repeated this experiment with several ice histories corresponding to several lithospheric strengths, but the results were similar to the result in Figure 7c. A few things can be observed. First, when the uncertainties in the true data are high, there is no change in the χ^2 values compared to the fully coupled results (Figure 6). Only for small (5–10%) uncertainties in the true data d^t there is a difference. The minimum is unaffected. However, the χ^2 values surrounding the minimum are higher. Interestingly, the χ^2 value for $De = 10^{22}$ Nm is also higher than with the full dynamical coupling, even though this value was used to calculate the ice history. This indicates the effect of adjusting the ice history only every 500 years instead of each time step.

[39] To further assess the influence of uncertainties in the ice model we calculated new true data d^t corresponding to a

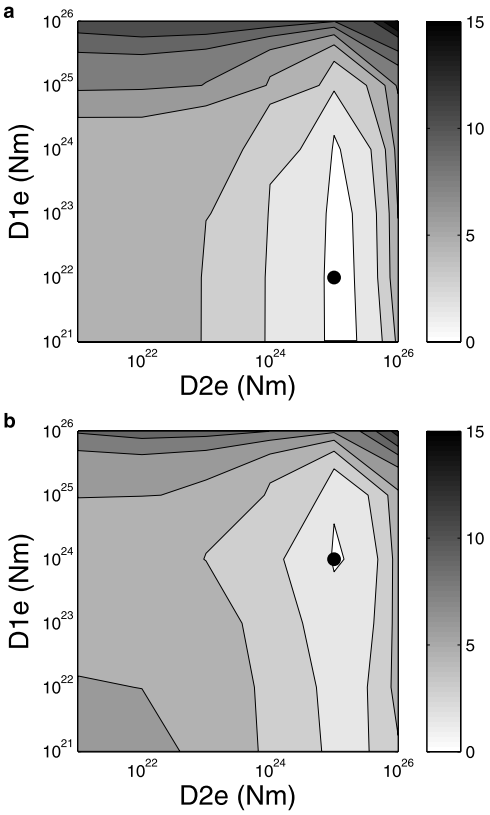

Figure 8. (a) The χ^2 distribution as a function of $D1e$ and $D2e$ for the case where the transition is in the center of the domain. (b) Similar to Figure 8a, but now the transition is moved 200 km to the west. The inversion, however, is still performed with the boundary between cells in the center of the domain, Figure 5. The contour lines are drawn at intervals of 1.5 starting at zero.

different climate. We then used the original climate to estimate the lithospheric strength De, this time with the full dynamical coupling between ice and Earth. In the case of a warmer true climate, this meant that the estimated values of De were assessed with an ice sheet that was too large. In the case of a colder true climate, the estimated ice sheets were too small. The resulting χ^2 values were very sensitive to the climate used to calculate the ice sheets. This is in agreement with the results of *Kaufmann et al.* [2005], who found that modeled crustal motions depended strongly on the specific ice history. The minimum value was shifted to a smaller value for De for the colder true climate, and to a larger value for De for the warmer true climate. This shift was associated with the bedrock adjustment near the ice margin. This is as expected since large ice sheets are generally not sensitive to the lithosphere in the center of the ice sheet.

[40] To assess the influence of uncertainties in the Earth model, we calculated new true data d^t corresponding to a different relaxation time τ and performed the experiment similarly to the different climate scenario, hence with the fully coupled model. The resulting χ^2 values were again very sensitive to this parameter. The resulting best estimate of the lithospheric strength was influenced, indicating the well known strong sensitivity of bedrock data to the viscosity of the mantle. This is in agreement with *Kaufmann and Wu* [2002], who found a trade-off between lithospheric structure and asthenospheric viscosity. The current lithosphere model however, is not adequate to study mantle viscosities. Therefore we assume the relaxation time is known.

5.2. Variable Strength Inversion

5.2.1. Fixed Location of Transition

[41] We continue the experiments with an inversion for variable strength of the lithosphere. Figure 5a again shows the geometry of the true model, which is the same as in the previous section. Instead of estimating a single value $D1e = D2e = De$, our objective is to find estimates for both a western value $D1e$ for the left part of the domain and an eastern value $D2e$ for the right part of the domain. We modeled data d^e with the full lithospheric model for several transitions in strengths from $D1e$ to $D2e$ and compared these data with the true data d^t with equation (11). The ice sheets were again calculated with the dynamical coupling between ice and Earth. Figure 8a shows the cost function χ^2 for each value of $D1e$ and $D2e$ for a 5% Gaussian noise level in the true data d^t. The minimum reflects the true values $D1$ and $D2$. The values for χ^2 are much closer to one than in Figure 6 (solid line), indicating that, as expected, this inversion leads to a better result.

[42] Figure 5 also shows the geometry of the next experiment. Figure 5a again depicts the geometry of the true model. The transition from weak (west) to strong (east) lithosphere no longer coincides with the highest point on the domain. Instead, the transition is shifted to the west by 200 km as indicated by the arrow and the thin solid line in Figure 5a. Otherwise all parameters remain unchanged. Figure 5b shows the geometry of the model we used to estimate $D1e$ and $D2e$. Notice that in this figure the transition still coincides with the highest point of the domain. Thus, in this experiment we have changed the true data d^t rather than changing the estimated data d^e. Since no combination of $D1e$ and $D2e$ equals the true geometry, we expect the χ^2 distribution from this inversion to be worse than the χ^2 distribution from the second experiment. Figure 8b shows the resulting χ^2 for the third experiment for a 5% Gaussian noise level. Indeed we see that the minimum value for χ^2 is slightly higher than in the previous experiment (1.5 compared to 1). More significantly however, the minimum is at different values for $D1e$ and $D2e$.

5.2.2. Moving Transition

[43] To examine this further, we performed the same experiment for varying locations of the transitions from weak to strong lithosphere. Furthermore, we added more noise to the true data d^t to address the robustness of the results. Figure 9a shows the minimum values of the individual χ^2 distributions as a function of location of the transition. The solid curve is the curve calculated with 5% noise in the true data d^t. The curves show that we only find a value χ^2 equal to one if the location of the transition used to estimate $D1e$ and $D2e$ agrees with the position of the transition used for the calculation of the true data. However, if we add more noise to the true data, the differences in the values of the misfit at their minima turn out to be insignificant. Each inversion is equally good. Figure 9b shows the corresponding allocated values of $D1e$ (west) and $D2e$ (east) as a function of location of the transition. Whereas each

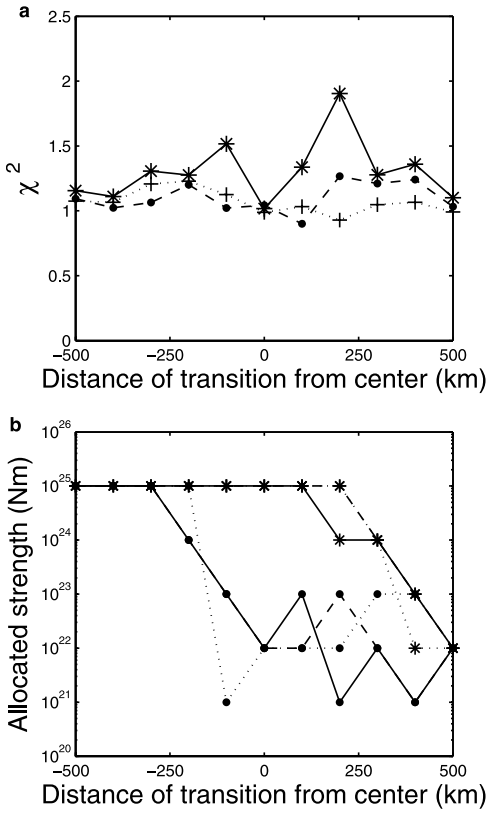

Figure 9. (a) Minimum of the χ^2 distributions for each of the locations of the transition for 5% noise (solid line), 10% noise (dash-dotted line), and 20% noise (dotted line). (b) Corresponding allocated strengths for the eastern half of the domain (stars) and the western half (solid circles) for the same noise levels.

estimate for $D1e$ and $D2e$ is equally good given the value of the misfit functions, the allocated values for the strength do change as a function of location of the transition (see also Figure 8b). If the transition lies more to the west, the allocated value in the west will be slightly larger.

[44] So, we cannot distinguish between different locations of the transition given the values of the misfit functions, but we do have different estimates for $D1e$ and $D2e$. Hence we conclude that we need some a priori information on the position of transitions in lithospheric strength from independent sources to estimate the rigidity of the lithosphere in the presence of lateral variations.

6. Discussion and Conclusions

[45] To resolve the strength of the lithosphere from sea level data we coupled a vertically integrated two-dimensional ice model to an Earth model. The Earth model consisted of an elastic lithosphere, where we incorporated lateral variations in lithospheric strength, with a single relaxation time due to the viscosity of the mantle.

[46] To illustrate the performance of the model we used a synthetic bedrock profile and a synthetic climate to model a characteristic ice sheet through an ice age cycle. The ice sheet had a maximum radius of about 600 km and was completely land based. The example demonstrated the importance for ice modeling of including the coupling between ice and Earth. Both the ice extent and the ice thicknesses were influenced resulting in significant differences in bedrock motions and ice volume. The ice volume differences resulting from different lithospheric strengths to calculate the isostatic bedrock adjustment, are about 10%.

[47] To exclude numerical instabilities, variations in D over several orders of magnitude are modeled over distances of 300 km. We cannot model local anomalies. However, since our objective is to have a good representation of ice on continental scales, this is not considered to be a drawback of this approach. For example, the Trans Antarctic Mountains, which served as inspiration for the examples in this paper and cover a transition in flexural rigidity over several orders of magnitude, are about 300 km wide.

[48] The inverse method presented in this paper yields comparable results to previous studies based on prescribed ice histories [e.g., *Kaufmann and Wu*, 2002; *Zhong et al.*, 2003]. Our results indicate that it is possible to constrain lateral variations in lithospheric strength from vertical bedrock motions, as long as there are data on both sides of the transition and a priori indications of the location. We stress that dynamical ice flow models are based on different assumptions and data sets than the generally used ice histories, such as ICE-3G. In addition, our inverse procedure, yields the best fitting ice history for the most likely lithospheric model.

[49] Our results show little sensitivity to Gaussian noise in the data, as long as the noise levels do not exceed about 20%. The algorithm is most sensitive to data from underneath former ice sheets. The method is sensitive to systematic biases due to for example insufficient knowledge on mantle viscosities, i.e., relaxation times, or past climate conditions. However, the current lithospheric model is not suitable to study the effect of viscosity structure of the mantle. For example, the model only uses one relaxation time, while viscoelastic Earth models generally have a spectrum of relaxation times. Therefore more sensitivity studies should be done in practical applications, for example Antarctica and Scandinavia.

[50] The model contains a purely elastic lithosphere. In reality, the lithosphere is probably viscoelastic and anomalies are more complicated than only a change in rigidity. The thin plate model remains a mechanical tool which is able to model the accurate deflection underneath loads. The elastic thickness has no proven connection to the actual thickness of the lithosphere. Thus the derived material properties are by no means the actual material properties of the lithosphere. Therefore geodynamical implications should be examined critically. For now, if the elastic properties can be resolved this is enough to correctly model the ice sheets.

[51] The method described here can be applied everywhere, provided that there are good constraints on the local climate as a function of time. Possible interesting applications include for example Antarctica, where indications exist for a large transition in lithospheric strength across the Trans Antarctic Mountains [e.g., *Bannister et al.*, 2003; *Stern and Ten Brink*, 1989]. Another possible application is Scandinavia where we expect an increase in lithospheric strength from the Atlantic coast toward cratonic Eurasia

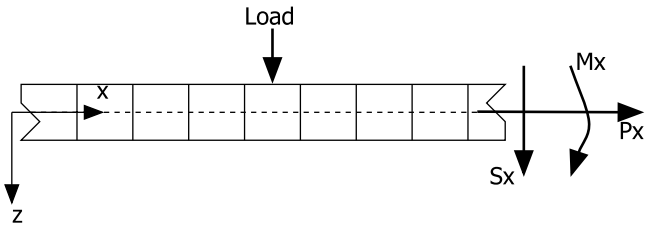

Figure A1. Geometry of a one-dimensional bending plate with directions of deformation and stress resultants.

[e.g., *Djomani et al.*, 1999; *Pérez-Gussinye and Watts*, 2005].

Appendix A: Thin Plate Theory

[52] Figure A1 shows a one-dimensional infinite plate subjected to a pressure load. We assume that the bending is cylindrical and that sections which are originally normal to the middle plane remain plane during deformation, thus only experience rigid translations and rotations. The total deformation can thus be described as

$$u(x,y,z) = u_0(x,y) - z\theta_x(x,y), \tag{A1}$$

$$v(x,y,z) = v_0(x,y) - z\theta_y(x,y), \tag{A2}$$

$$w(x,y) = w_0(x,y), \tag{A3}$$

where u_0, v_0 and w_0 are rigid translations and $\theta_{x,y}$ are rotations of the normals to the middle plane.

[53] We finally assume that the thickness of the plate is small compared to the horizontal dimensions of the load. We can then assume that the vertical shear forces are small [*Zienkiewicz and Taylor*, 2000].

[54] Figure A1 shows the stress resultants M_x (bending moment), S_x (shear stress) and P_x (normal stress). These stress resultants can be calculated using

$$M_x = -\int_{-h/2}^{h/2} z\,\sigma_{xx}\,\mathrm{d}z, \tag{A4}$$

$$S_x = \int_{-h/2}^{h/2} \sigma_{xz}\,\mathrm{d}z, \tag{A5}$$

$$P_x = \int_{-h/2}^{h/2} \sigma_{xx}\,\mathrm{d}z. \tag{A6}$$

where the integration is over the entire thickness of the plate h. The bending moment M_x can be regarded as a leverage, the other resultants are total stresses.

[55] In two dimensions, in addition to M_x, S_x and P_x, we also have M_y, S_y, P_y,P_{xy} and a twisting moment M_{xy}. These are defined similarly to M_x, S_x and P_x.

[56] We can solve for the deformation by writing down the equilibrium equations. These equations can be formulated by integration of the local equilibrium equations [*Zienkiewicz and Taylor*, 2000; *Van der Veen*, 1999]:

$$\int_{-h/2}^{h/2} \left[\frac{\partial\sigma_{xx}}{\partial x} + \frac{\partial\sigma_{xy}}{\partial y} + \frac{\partial\sigma_{xz}}{\partial z}\right]\mathrm{d}z = \frac{\partial P_x}{\partial x} + \frac{\partial P_{xy}}{\partial y} = 0, \tag{A7}$$

$$\int_{-h/2}^{h/2} \left[\frac{\partial\sigma_{yx}}{\partial x} + \frac{\partial\sigma_{yy}}{\partial y} + \frac{\partial\sigma_{yz}}{\partial z}\right]\mathrm{d}z = \frac{\partial P_{xy}}{\partial x} + \frac{\partial P_y}{\partial y} = 0, \tag{A8}$$

$$\int_{-h/2}^{h/2} \left[\frac{\partial\sigma_{xz}}{\partial x} + \frac{\partial\sigma_{yz}}{\partial y} + \frac{\partial\sigma_{zz}}{\partial z}\right]\mathrm{d}z = \frac{\partial S_x}{\partial x} + \frac{\partial S_y}{\partial y} + q = 0, \tag{A9}$$

where q is the loading. Notice that in q not only the load, but also the buoyancy at the bottom of the plate is incorporated as $q = q_{load} - q_{buoy}$, where $q_{buoy} = \rho_m g w$, where ρ_m is the density of the mantle.

[57] Three equations are insufficient to solve the deformation problem, so we use the bending moments:

$$\int_{-h/2}^{h/2} z\left[\frac{\partial\sigma_{xx}}{\partial x} + \frac{\partial\sigma_{xy}}{\partial y} + \frac{\partial\sigma_{xz}}{\partial z}\right]\mathrm{d}z = \frac{\partial M_x}{\partial x} + \frac{\partial M_{xy}}{\partial y} + S_x = 0, \tag{A10}$$

$$\int_{-h/2}^{h/2} z\left[\frac{\partial\sigma_{yx}}{\partial x} + \frac{\partial\sigma_{yy}}{\partial y} + \frac{\partial\sigma_{yz}}{\partial z}\right]\mathrm{d}z = \frac{\partial M_y}{\partial y} + \frac{\partial M_{xy}}{\partial x} + S_y = 0. \tag{A11}$$

The equations containing P describe the horizontal deformation and decouple from the rest of the equations.

[58] Since the vertical normal stress in the plate is small compared to the other stresses [*Zienkiewicz and Taylor*, 2000], it is neglected except for the formulation of the upper and lower boundary conditions, where we need the loading pressure. We assume all deformation is elastic, which results in the following expression for the stress tensor

$$\boldsymbol{\sigma} = \frac{E}{1+\nu}\begin{pmatrix} \frac{1}{1-\nu}\left(\epsilon_{xx} + \nu\epsilon_{yy}\right) & \epsilon_{xy} & \epsilon_{xz} \\ \epsilon_{xy} & \frac{1}{1-\nu}\left(\nu\epsilon_{xx} + \epsilon_{yy}\right) & \epsilon_{yz} \\ \epsilon_{xz} & \epsilon_{yz} & 0 \end{pmatrix}, \tag{A12}$$

where E and ν are Young's modulus and Poisson's ratio. The deformation tensor ϵ_{ij} is defined as

$$\epsilon_{ij} = \frac{1}{2}\left(\frac{\partial u_i}{\partial x_j} + \frac{\partial u_j}{\partial x_i}\right). \tag{A13}$$

[59] If we now integrate the expressions for the stress resultants to find the resulting expressions with deformation, we find $\theta \approx \nabla w$, and this results in

$$(\mathbf{L}\nabla)^T \mathbf{D}'\mathbf{L}\nabla w - q = 0, \tag{A14}$$

where $(\mathbf{L}\nabla)$ is given by

$$(\mathbf{L}\nabla) = \left[\frac{\partial^2}{\partial x^2} \quad \frac{\partial^2}{\partial y^2} \quad 2\frac{\partial^2}{\partial x \partial y} \right]^T. \tag{A15}$$

The matrix $\mathbf{D}'$ is given by

$$\mathbf{D}' = D \begin{bmatrix} 1 & \nu & 0 \\ \nu & 1 & 0 \\ 0 & 0 & (1-\nu)/2 \end{bmatrix}, \tag{A16}$$

where D is called the flexural rigidity and given by

$$D = \frac{Eh^3}{12(1-\nu^2)}. \tag{A17}$$

If we now assume the flexural rigidity or bending stiffness D' to be constant throughout the medium, we find the equation widely used for the calculation of flexure in geophysics

$$D\left(\frac{\partial^4 w}{\partial x^4} + 2\frac{\partial^4 w}{\partial x^2 \partial y^2} + \frac{\partial^4 w}{\partial y^4}\right) - q = 0. \tag{A18}$$

This equation can be solved analytically [e.g., *Turcotte and Schubert*, 2002; *Van der Veen*, 1999; *Le Meur and Huybrechts*, 1996; *Brotchie and Silvester*, 1969].

[60] For situations where D is not constant however, the equation is given by [see also *Van Wees and Cloetingh*, 1994]

$$\frac{\partial^2}{\partial x^2}\left(D\frac{\partial w^2}{\partial x^2}\right) + \nu\frac{\partial^2}{\partial y^2}\left(D\frac{\partial^2 w}{\partial x^2}\right) + \nu\frac{\partial^2}{\partial x^2}\left(D\frac{\partial^2 w}{\partial y^2}\right) + \frac{\partial^2}{\partial y^2}\left(D\frac{\partial^2 w}{\partial y^2}\right) + 2(1-\nu)\frac{\partial^2}{\partial x \partial y}\left(D\frac{\partial^2 w}{\partial x \partial y}\right) - q = 0. \tag{A19}$$

[61] **Acknowledgments.** The calculations were performed on the RADON cluster of IMAU, which was partly funded by the Utrecht Center for Geosciences. This work was financed by the Spinoza Award of NWO of J. Oerlemans. We thank John Wahr and an anonymous reviewer for their valuable comments.

References

Bannister, S., J. Yu, B. Leitner, and B. Kennett (2003), Variations in crustal structure across the transition from West to East Antarctica, Southern Victoria Land, *Geophys. J. Int.*, *155*, 870–884.

Braitenberg, C., J. Ebbing, and H. Gotze (2002), Inverse modelling of elastic thickness by convolution method: The eastern Alps as a case example, *Earth Planet. Sci. Lett.*, *202*, 387–404.

Brotchie, J., and R. Silvester (1969), On crustal flexure, *J. Geophys. Res.*, *74*(22), 5240–5252.

Darbyshire, F., T. Larsen, K. Mosegaard, T. Dahl-Jensen, O. Gudmundsson, T. Bach, S. Gregersen, H. Pedersen, and W. Hanka (2004), A first detailed look at the Greenland lithosphere and upper mantle using Rayleigh wave tomography, *Geophys. J. Int.*, *158*, 267–286.

Di Donato, G., L. Vermeersen, and R. Sabadini (2000), Sea-level changes, geoid and gravity anomalies due to Pleistocene deglaciation by means of multilayered, analytical Earth models, *Tectonophysics*, *320*, 409–418.

Djomani, Y. P., J. Fairhead, and W. Griffin (1999), The flexural rigidity of Fennoscandia: Reflection of the tectonothermal age of the lithospheric mantle, *Earth Planet. Sci. Lett.*, *174*, 139–154.

Hutter, K. (1983), *Theoretical Glaciology*, Springer, New York.

Huybrechts, P. (1992), The Antarctic ice sheet and environmental change: A three-dimensional modelling study, *Rep. Polar Res.*, *99*, 241 pp.

Huybrechts, P., T. Payne, and The EISMINT Intercomparison Group (1996), The EISMINT benchmarks for testing ice-sheet models, *Ann. Glaciol.*, *23*, 1–12.

Kaufmann, G., and P. Wu (2002), Glacial isostatic adjustment in Fennoscandia with a three-dimensional viscosity structure as an inverse problem, *Earth Planet. Sci. Lett.*, *197*, 1–10.

Kaufmann, G., P. Wu, and G. Li (2000), Glacial isostatic adjustment in Fennoscandia for a laterally heterogeneous Earth, *Geophys. J. Int.*, *143*, 262–273.

Kaufmann, G., P. Wu, and E. Ivins (2005), Lateral viscosity variations beneath Antarctica and their implications on regional rebound motions and seismotectonics, *J. Geodyn.*, *39*, 165–181.

Le Meur, E., and P. Huybrechts (1996), A comparison of different ways of dealing with isostasy: Examples from modelling the Antarctic ice sheet during the last glacial cycle, *Ann. Glaciol.*, *23*, 309–317.

Mahaffy, M. (1976), A three-dimensional numerical model of ice sheets: Tests on the Barnes ice cap, Northwest Territories, *J. Geophys. Res.*, *81*(6), 1059–1066.

Milne, G., J. Mitrovica, and D. Schrag (2002), Estimating past continental ice volume from sea-level data, *Quat. Sci. Rev.*, *21*, 361–376.

Pérez-Gussinye, M., and A. Watts (2005), The long-term strength of Europe and its implications for plate-forming processes, *Nature*, *436*, 381–384.

Stern, T., and U. Ten Brink (1989), Flexural Uplift of the Transantarctic Mountains, *J. Geophys. Res.*, *94*(B8), 10,315–10,330.

Turcotte, D., and G. Schubert (2002), *Geodynamics*, 2nd ed., Cambridge Univ. Press, New York.

Tushingham, A., and W. Peltier (1991), Ice-3G: A new global model of late Pleistocene deglaciation based upon geophysical predictions pf post-glacial relative sea level change, *J. Geophys. Res.*, *96*(B3), 4497–4523.

van den Berg, J., R. S. W. van de Wal, and J. Oerlemans (2006), Effects of spatial discretization in ice-sheet modelling, *J. Glaciol.*, in press.

Van der Veen, C. (1999), *Fundamentals of Glacier Dynamics*, A. A. Balkema, Brookfield, Vt.

Van Wees, J., and S. Cloetingh (1994), A finite-difference technique to incorporate spatial variations in rigidity and planar faults into 3-D models for lithospheric flexure, *Geophys. J. Int.*, *117*, 179–195.

Vermeersen, L., and R. Sabadini (1999), Polar wander, sea-level variations and ice age cycles, *Surv. Geophys.*, *20*, 415–440.

Wolf, D. (1993), The changing role of the lithosphere in models of glacial isostasy: A historical review, *Global Planet. Change*, *8*, 95–106.

Zhong, S., A. Paulson, and J. Wahr (2003), Three-dimensional finite-element modelling of Earth's viscoelastic deformation: Effects of lateral variations in lithospheric thickness, *Geophys. J. Int.*, *155*, 679–695.

Zienkiewicz, O., and R. Taylor (2000), *The Finite Element Method*, vol. 2, *Solid Mechanics*, 5th ed., Butterworth-Heinemann, Elsevier, New York.

J. Oerlemans, R. S. W. van de Wal, and J. van den Berg, Institute for Marine and Atmospheric Research, University of Utrecht, Princetonplein 5, NL-3584CC Utrecht, Netherlands. (j.vandenberg@phys.uu.nl)